INSTITUTE OF PHYSICS PUBLISHING and IAEA NUCLEAR FUSION
Nucl. Fusion **42** (2002) 66–75 PII: S0029-5515(02)32320-2

Local physics basis of confinement degradation in JET ELMy H mode plasmas and implications for tokamak reactors

R.V. Budny[1], B. Alper[2], D.N. Borba[2,3], J.G. Cordey[2], D.R. Ernst[1], C. Giraud[2], C.W. Gowers[2], K. Gunther[2], T.S. Hahm[1], G.W. Hammett[1], N.C. Hawkes[2], L.D. Horton[4], G. Saibene[5], R. Sartori[5], E.J. Synakowski[1], M.G. von Hellermann[6], K.-D. Zastrow[2]

JET Joint Undertaking, Abingdon, Oxfordshire, United Kingdom

[1]Princeton Plasma Physics Laboratory, Princeton University, Princeton, New Jersey, United States of America
[2]Euratom/UKAEA Fusion Association, Abingdon, Oxfordshire, United Kingdom
[3]Euratom–Instituto Superior Técnico Association, Lisbon, Portugal
[4]Max-Planck-Institut für Plasmaphysik, Garching, Germany
[5]EFDA Close Support Unit, Max-Planck-Institut für Plasmaphysik, Garching, Germany
[6]FOM Institute for Plasma Physics Rijnhuizen, Nieuwegein, Netherlands

E-mail: budny@princeton.edu

Received 4 October 2000, accepted for publication 9 May 2001
Published 30 January 2002
Online at stacks.iop.org/NF/42/66

Abstract
First results of gyrokinetic analysis of JET ELMy H mode plasmas are presented. ELMy H mode plasmas form the basis of conservative performance predictions for tokamak reactors of the size of ITER. Relatively high performance for long durations has been achieved and the scaling appears to be favourable. It will be necessary to sustain low Z_{eff} and high density for high fusion yield. The article studies the degradation in confinement and the increase in the anomalous heat transport observed in two JET plasmas: one with an intense gas puff and the other with a spontaneous transition from type I to III ELMs at the heating power threshold. Linear gyrokinetic analysis gives the growth rate γ_{lin} of the fastest growing modes. The flow shearing rate $\gamma_{E\times B}$ and γ_{lin} are large near the top of the pedestal. Their ratio decreases approximately at the time when the confinement degrades and the transport increases. This suggests that tokamak reactors may require intense toroidal or poloidal torque input to maintain sufficiently high $\gamma_{E\times B}/\gamma_{lin}$ near the top of the pedestal for high confinement.

PACS numbers: 52.55.Fa, 52.30.Gz

1. Introduction

The H mode regime in the ELM phase is favoured for large, conventional tokamak reactors since it has obtained enhanced performance for long durations. Deuterium–tritium experiments in JET ELMy plasmas have achieved $Q_{dt} = 0.2$ [1]; however, the confinement in similar plasmas tends to degrade as the density is pushed towards the Greenwald limit by gas puffing [2] or pellet injection [3]. This degradation is often associated with the transition from type I to III ELMs [4]. Experiments in some other tokamaks and recently in JET have produced ELMy H mode plasmas with high confinement near the Greenwald limit, but not yet with DT plasmas.

Toroidal non-linear theory indicates that the microturbulence which is believed to cause anomalous transport is reduced by shear in the $\boldsymbol{E}\times\boldsymbol{B}$ rotation (more specifically, the $\boldsymbol{E}\times\boldsymbol{B}/RB_{pol}$ rotation induced by E_r), quantified by the shearing rate $\gamma_{E\times B}$, defined below [5]. A measure of this reduction can be given by the ratio of $\gamma_{E\times B}$ and the linear growth rate γ_{lin} of the most unstable toroidal mode with high toroidal mode number. Simulations indicate that where this ratio is less than $\simeq$1, the plasma is expected to have reduced confine-

ment [6]. This effect can be summarized in

$$\chi_i = \chi_0 \max\left(0, \left[1 - \alpha_{exb}\,\frac{\gamma_{E\times B}}{\gamma_{lin}}\right]\right) \qquad (1)$$

where χ_0 gives the transport in the hypothetical plasma with the same conditions, except with zero $\gamma_{E\times B}$, and α_{exb} is a constant of order 1.

There is experimental evidence that $\gamma_{E\times B}$ can have an influence on the confinement. Some plasma regimes, such as those with weak or reversed magnetic shear in JET and other tokamaks, have achieved considerably lower transport transiently, with ion thermal and particle transport near the neoclassical level. Generally these regimes have relatively large $\gamma_{E\times B}$, with magnitude significantly larger than the computed maximum growth rate, γ_{lin}, of high n toroidal modes associated with microturbulence. An example of $\gamma_{E\times B}$ and γ_{lin} analysis for a JET 'optimized magnetic shear' plasma is given in Ref. [7].

Experiments where $\gamma_{E\times B}$ is varied by changing the applied torque also suggest that $\boldsymbol{E}\times\boldsymbol{B}$ shear plays a fundamental role in governing the confinement in these regimes [8, 9]. There is also experimental evidence that modifying the rotation dominated $\boldsymbol{E}\times\boldsymbol{B}$ shear can influence the local transport in a continuous fashion, even when transport rates far exceed the neoclassical values [10–12].

JET ELMy H mode plasmas heated by NBI have large toroidal rotation rates f_{tor}, with Mach numbers near unity in the centre. Empirical fits to the dimensionless heat transport ($\chi_i/(\Omega_i L_{Ti}^2)$), normalized by the local ion gyrofrequency Ω_i and T_i scale length ($L_{Ti} \equiv -T_i/(\partial T_i/\partial r)$), indicate a reduction with increasing Mach number [13], further suggesting that $\gamma_{E\times B}$ plays a role.

This article studies the energy transport and γ_{lin} in JET ELMy H mode plasmas with NBI heating and degradation in confinement. Evidence is presented that, at least in these NBI heated plasmas, $\gamma_{E\times B}$ plays a role in the degradation of confinement and the increase in local heat transport. Energy confinement degradation occurs, in this picture, as a consequence of changes in the beam induced rotation at high density causing the reduction of $\gamma_{E\times B}/\gamma_{lin}$.

The results suggest that if tokamak power producing reactors require high confinement in the ELMy H mode regime, a large $\gamma_{E\times B}/\gamma_{lin}$ will be required. An external source of $\gamma_{E\times B}$ near the top of the pedestal may be sufficient to obtain high confinement.

A brief summary was presented at the 2000 IAEA Fusion Energy Conference [14]. A recent reanalysis of the charge exchange geometry has resulted in corrections to data for the lower power plasma. This does not change our conclusions.

2. Data

Parameters for the two JET plasmas are summarized in Table 1. Both plasmas experience a decrease in confinement, as seen in the W_{dia}, H_{89} and H_{97} traces in Fig. 1. One plasma is dominantly tritium, with intense gas puffing to achieve high density, making it the more reactor relevant of the two. The line averaged electron density $\bar{n}_e$ increased to 87% of the Greenwald limit ($I_p/\pi a^2$ (MA m^{-2})) as a result of T_2 gas injection into the SOL at a rate of 1.3×10^{22} atoms/s. A relatively low Z_{eff} was achieved ($\simeq$ 1.2 in the core). The Troyon normalized pressure β_N reached 1.53 just as the intense puffing started, then decreased gradually. The H mode started with a brief phase of 'transition type III' ELMs at 17.1 s, followed by an ELM free phase, during which the puffing started, evolving to type I ELMs at 18.5 s, and then gradually, at around 19.2–19.9 s, to 'density limit' type III ELMs. More details of this plasma and comparisons with similar plasmas are given in Ref. [2].

The other plasma is dominantly deuterium, with sufficiently low NBI power to be at the threshold for the transition from type I to III ELMs. The plasma has an ELM free H mode phase from 18.3 to 20.8 s, followed by a type I phase until 21.6 s, and then by a type III phase ending at 25.6 s. A marked loss of confinement is seen in the line integrated electron density and stored energy traces during the type III phase. The confinement recovers during an ELM free phase near the end of the NBI. Although it is less reactor relevant than the first, this plasma provides evidence for the theoretical understanding of confinement degradation.

One of the main results of this article is that the suppression ratio $\gamma_{E\times B}/\gamma_{lin}$ near the top of the pedestal tends to decrease to low values (reduction of suppression) when W_{dia} and the confinement decrease. The time evolutions of this ratio at several radii near the top of the pedestal is shown in the bottom panels of Fig. 1. The times chosen for the gyrokinetic analysis are indicated by the vertical dashed lines in the figure. Some radii show a moderate decrease in the suppression ratio comparable to the magnitude of the decrease in W_{dia} with increasing density.

The thermal energy densities, shown in Fig. 2, tend to shift up or down with the global W_{dia}, shown in Fig. 1, i.e. the profiles are 'stiff', suggesting that the energy diffusivity does not appear to depend sensitively on temperature. The vertical dashed lines show the approximate location of the top of the pedestal, as indicated by the light detection and ranging (LIDAR) measurements of n_e and T_e [15].

The n_e profiles used for the modelling were extrapolated from the LIDAR measurements using chordal densities measured by interferometry. The profiles change significantly in time with the energy confinement of the two plasmas: increasing in 43002 and decreasing in 49687.

Profiles for T_i, Z_{eff} and the toroidal rotation rate f_{tor} were measured during the NBI phase using charge exchange spectroscopy [16]. The profiles of Z_{eff} are derived from measurements of the impurity densities. For 43002, the He, Be and C impurity densities were measured. For 49687, only the dominant C impurity density was measured. The x variable used in the figures is $x \equiv \sqrt{\text{normalized toroidal flux}}$, which is roughly equal to the normalized minor radius of the flux surface, r/a. The mapping of the measured data to x was done using the TRANSP code, discussed in the next section. The measurements extend to a major radius near $R = 3.75$ m, i.e. $x \simeq 0.88$.

The T_i data are extended out towards the edge using measurements from an edge spectroscopy system [17]. Examples are shown in Fig. 3. Near the midradius, the T_i profiles tend to be stiff. This is indicated in several ways. The profiles of the major radius normalized gradient scale length are relatively constant in time, as shown in Fig. 4. The ion heat

Table 1. Summary of plasma parameters

Shot number (year)	43002 (1997)	49687 (1999)
Type I → III transition	Forced by gas puff	Spontaneous
Time traces	Fig. 1(a)	Fig. 1(b)
R/a (m)	2.88/0.95	2.94/0.90
B_{tor} (T)	2.8	2.0
I_p (MA)	2.6	1.9
P_{NB} (MW)	8 (T^0) + 3 (D^0)	5 (D^0)
n_e	Increase	Large decrease
$n_e(0)/\langle n_e\rangle$	0.9 → 1.1	∼1.3
$\bar{n}_e/\bar{n}_{Greenwald}$	→ 0.85	0.75 → 0.35
β_n	1.53	1.9 → 0.8
f_{tor}	Increase	Large decrease
τ_E	20% decrease	50% decrease
χ_i, χ_{eff}	Slight increase near pedestal	Factor of 2–3 increase

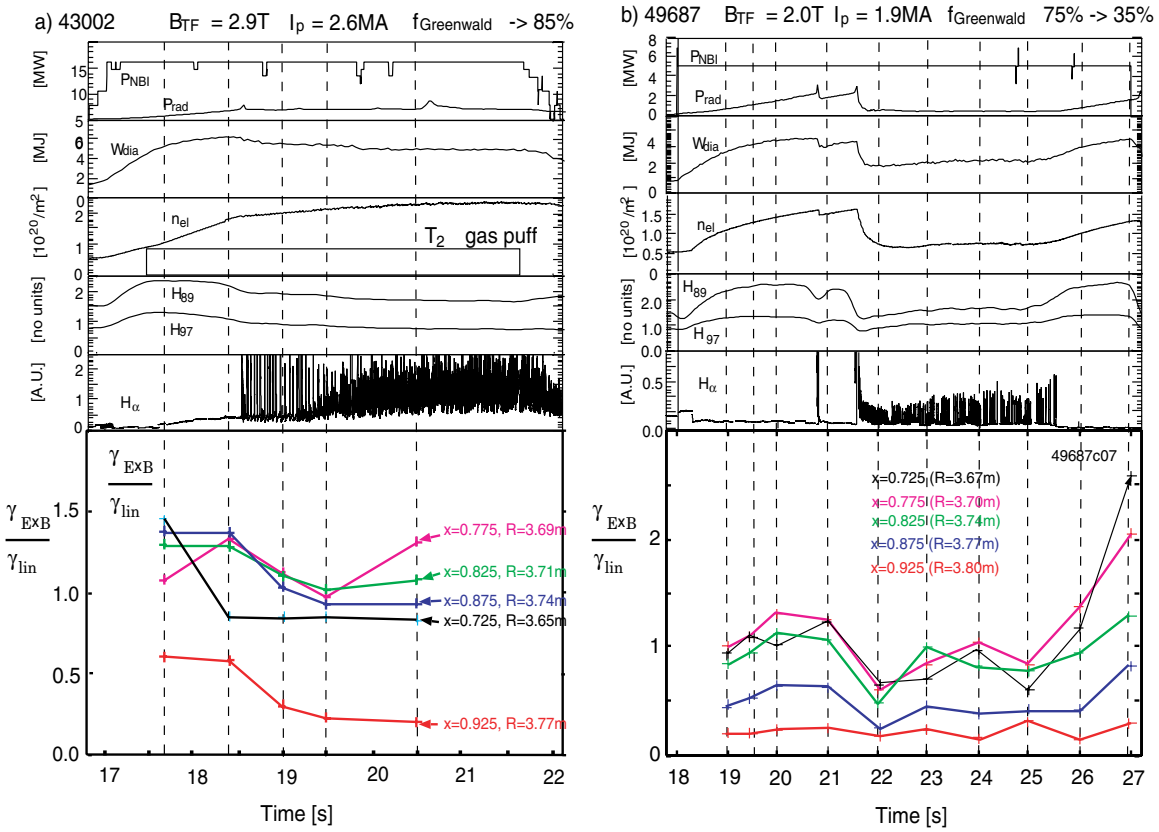

Figure 1. Waveforms: (a) shot 43002 with intense gas puff and (b) shot 49687 with a spontaneous type I → III ELM transition; bottom: microturbulence suppression ratio at several radii near the top of the pedestal. Vertical dashed lines indicate analysis times.

conduction coefficient χ_i tends to increase rapidly as R/L_{Ti} increases past a critical value (in the vicinity of $R/L_{Ti} \simeq 5$). As shown below, R/L_{Ti} appears to be governed by a critical gradient, R/L_T^{crit}, over much of the profile. The measured toroidal rotation f_{tor} behaves very similarly to T_i, as shown in Fig. 5.

Below we analyse the heat transport in the plasmas, and correlate the increase in transport and degradation of confinement with decreases in $\gamma_{E\times B}/\gamma_{lin}$. MHD also can increase transport and degrade confinement. For 43002, the mode with the largest measured amplitude, having $n = 2$, is first observed in the magnetic probes after 18.5 s, when the plasma transitions from ELM free to type I ELMs. This mode has a maximum amplitude of $\delta B = (2\text{–}3) \times 10^{-4}$ T at the probe location and lasts until 22.0 s. The amplitude decreases during the 3.5 s period in which the mode is observed, and by 21.5 s the amplitude is $\delta B < 6 \times 10^{-5}$ T. The frequency of the perturbation decreases from 14 to 7 kHz owing to the decrease in the plasma toroidal rotation frequency. This type of instability can degrade the plasma energy confinement, but in this plasma the amplitude is small and decreasing when the confinement degradation is increasing, and thus it does not appear to be the main cause of the degradation. The fit to the data from the nine Mirnov coil array gives $(m, n) = (3, 2)$ for this mode. Fourier analysis of the fast electron cyclotron emission (ECE) channels gives the outer major radius location of the mode at 20.5 s at 3.30–3.42 m. This is close to the region where TRANSP calculates $q = 1.5$, and is deeper inside the plasma than the region where the calculated microinstability linear growth is positive.

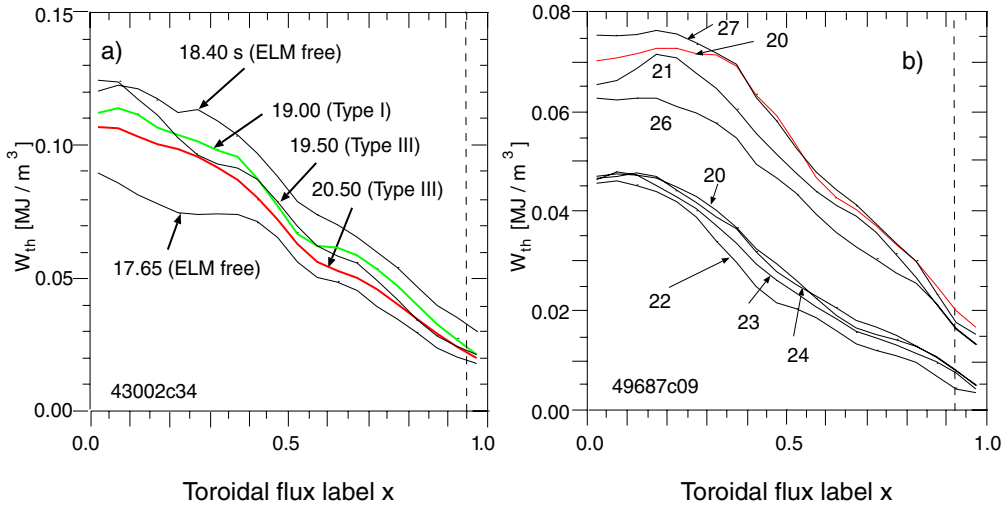

Figure 2. Thermal energy densities mapped to the toroidal flux label.

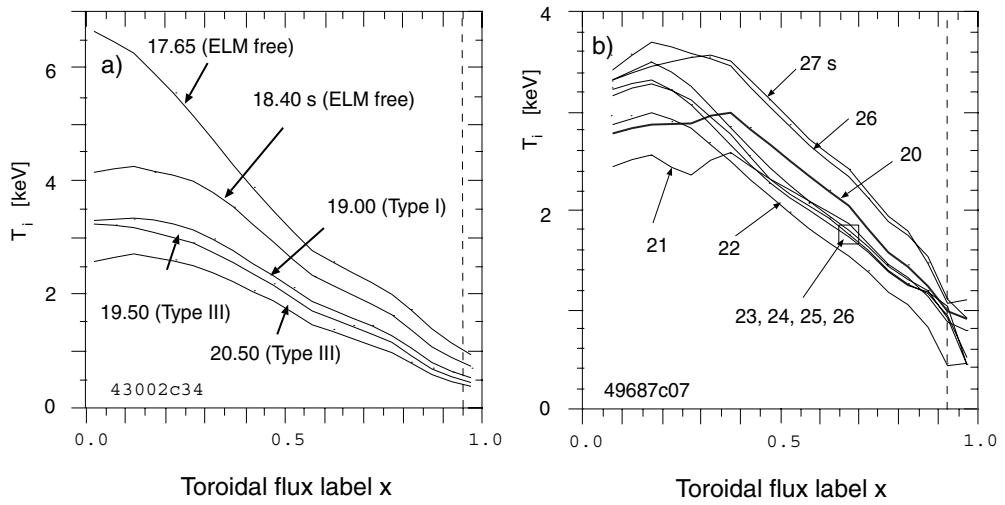

Figure 3. Measured T_i mapped to the toroidal flux label.

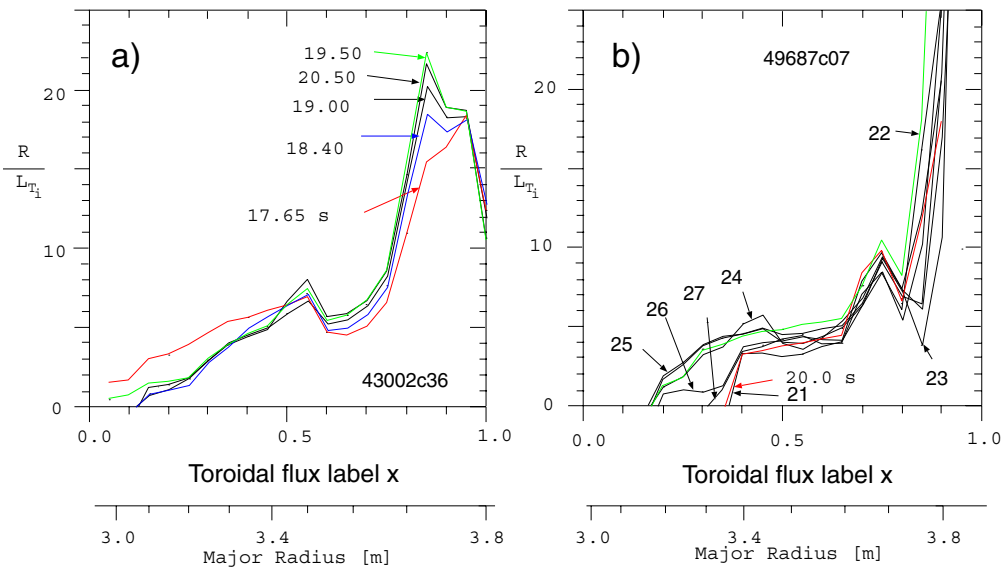

Figure 4. Measured R/L_{Ti} mapped to the toroidal flux label.

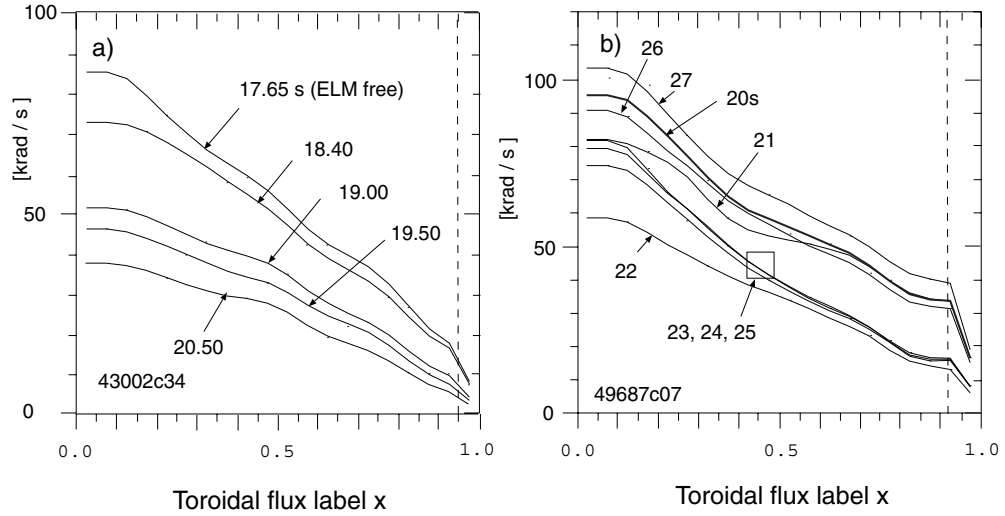

Figure 5. Measured toroidal rotation frequency mapped to the toroidal flux label.

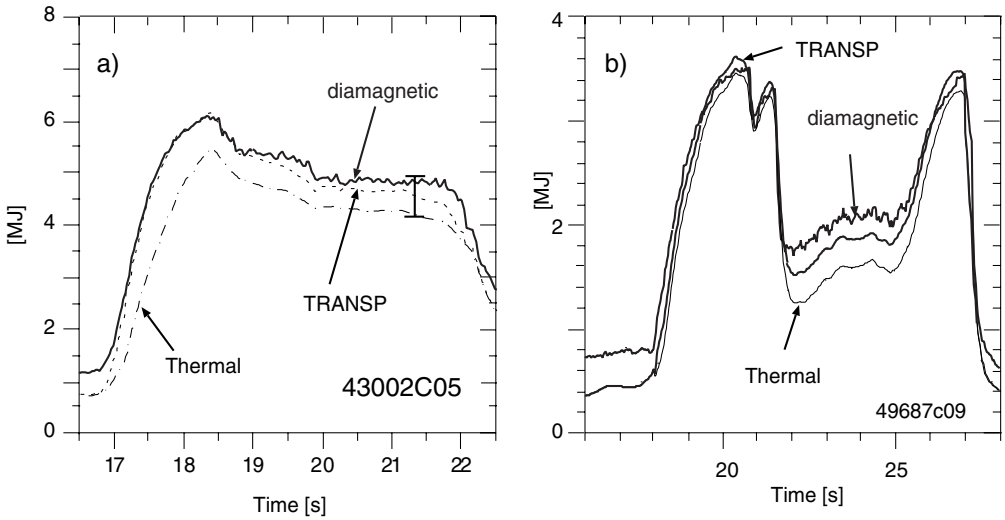

Figure 6. Comparison of measured and TRANSP calculated stored energies.

3. TRANSP analysis

The TRANSP plasma analysis code [18] is used to analyse the heat transport and $\gamma_{E\times B}$. TRANSP is an interpolative code, making maximal use of measurements and minimal assumptions. In order to obtain relatively smooth, quasi-steady-state profiles for χ_i and $\gamma_{E\times B}$, and to average over channel to channel systematic variations, the profiles were smoothed in time with an averaging window of up to 200 ms. Sawteeth change profiles near the centre, and ELMs change profiles near the pedestal. The time averaging of the data removes information about the sawteeth and ELMs. This article focuses on quasi-steady-state phenomena, with gyrokinetic analysis at relatively few points in time, so the sawtooth and ELM time dependence is ignored.

TRANSP simulates the measured stored energy accurately, as shown in Fig. 6. This increases the credibility of the TRANSP calculations of the fast ion energy density, power and torque deposition, and heat transport.

The NBI torque deposition is shown in Fig. 7. For 43002, as the density increases, both the NBI heating and the torque decrease in the centre as the penetration decreases with increasing density. Most of the NBI sources for this plasma had a full energy component of 150 keV. These decreases of heating and torque in the centre correlate with the reduction of the central T_i and f_{tor} shown in Figs 3–5. The flattening of the f_{tor} profile causes the reduction of $\gamma_{E\times B}$, discussed below. For 49687, with a decrease in density, the NBI torque and heat deposition show little change in shape.

The heat transfer χ_i for 43002 (Fig. 8(a)) decreases during the ELM free phase until the start of the T_2 puff. During the puff, the values change relatively little in the core region ($R < 3.6$ m); however, outside $R = 3.6$ m the values increase, especially near the pedestal, and after the transition to type III ELMs. For 49687, a large increase in χ_i is seen across most of the profile when the energy confinement degrades. When the confinement recovers at around 26 s, χ_i decreases. The effective ion and electron heat χ_{eff} shows similar trends. The correspondence between the variable x and the major radius R is shown in the figure.

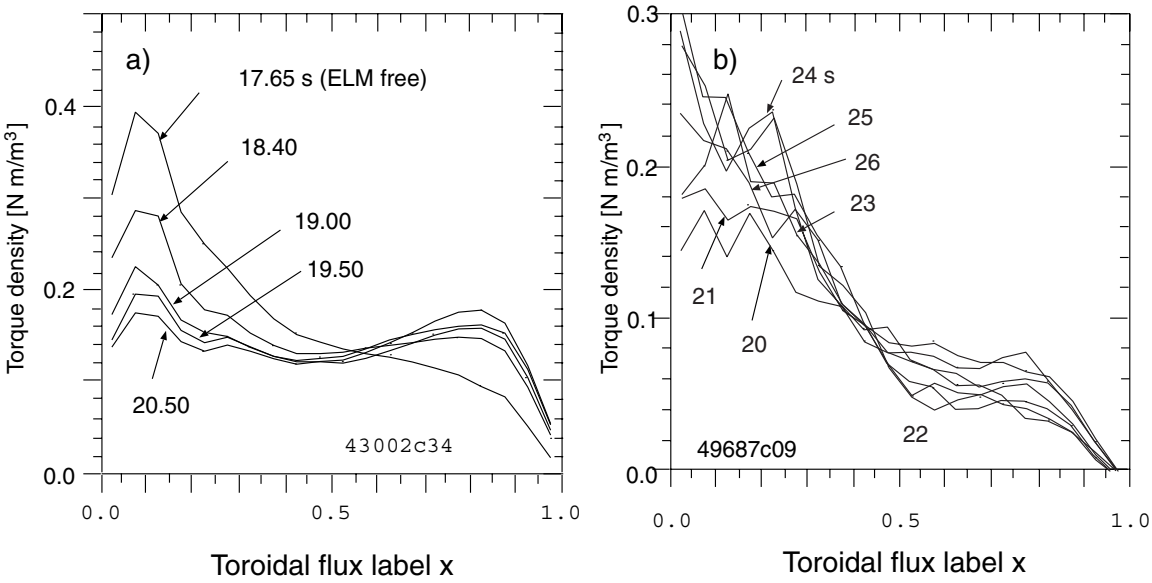

Figure 7. NBI torque density profiles.

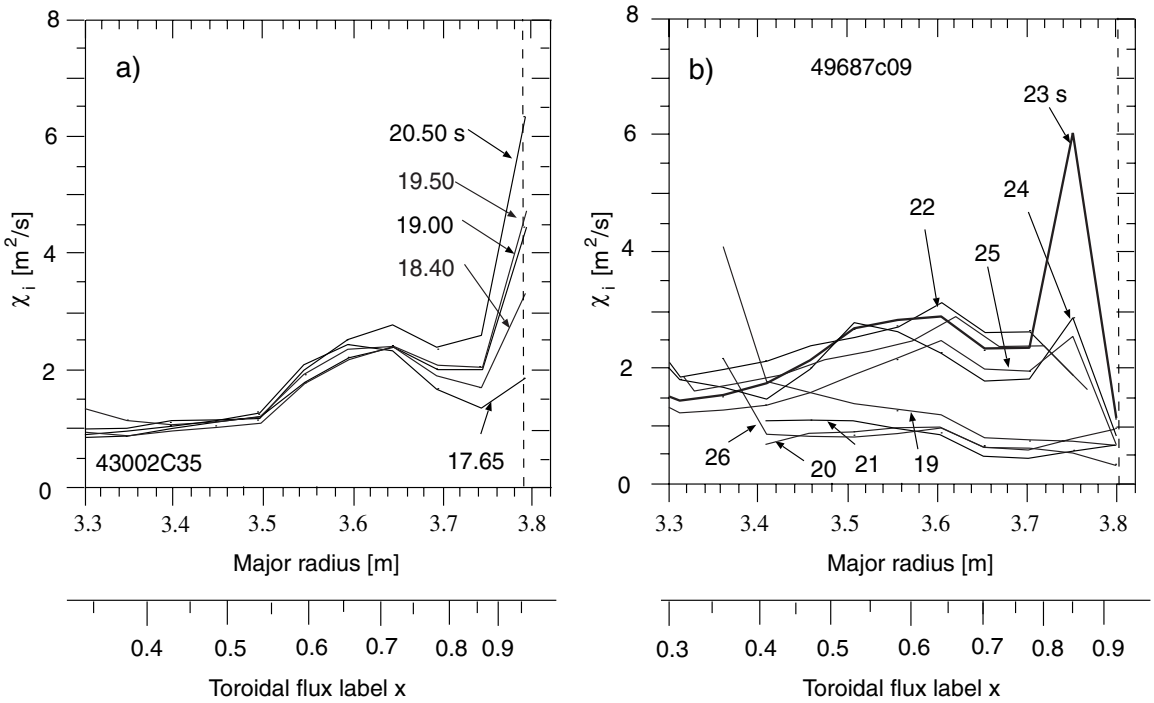

Figure 8. Thermal ion energy transport coefficient versus major radius and toroidal flux label x. Vertical dashed lines indicate approximate location of the top of the pedestal.

4. Flow shear and growth rates

The profile of the radial electric field E_r is calculated from the force balance of the trace carbon impurity:

$$\nabla(p) = eZ(E + v \times B) \tag{2}$$

$$E_r = v_{tor} B_{pol} - v_{pol} B_{tor} + \frac{1}{Z_{imp} e n_{imp}} \nabla(p_{imp}) \tag{3}$$

where n_{imp} and p_{imp} are the measured impurity density and pressure ($\propto n_{imp} T_{imp}$), and Z_{imp} is the charge of the impurity (6 here). B_{pol} is calculated by TRANSP solving the poloidal field diffusion. Since the poloidal rotation profile is not measured, we use a neoclassical expression to compute v_{pol} [19, 20]. In general, for JET ELMy H mode plasmas, the impurity pressure is a very small contribution to E_r, except possibly in the pedestal and edge. Not enough plasma measurements are available in the pedestal for us to study details in that region, so we focus on the region between the core and the top of the pedestal. Since the NBI in JET is unidirectional (co), NBI heated ELMy plasmas have $\gamma_{E\times B}$ and E_r dominated by the toroidal rotation term. The profiles show little change in shape

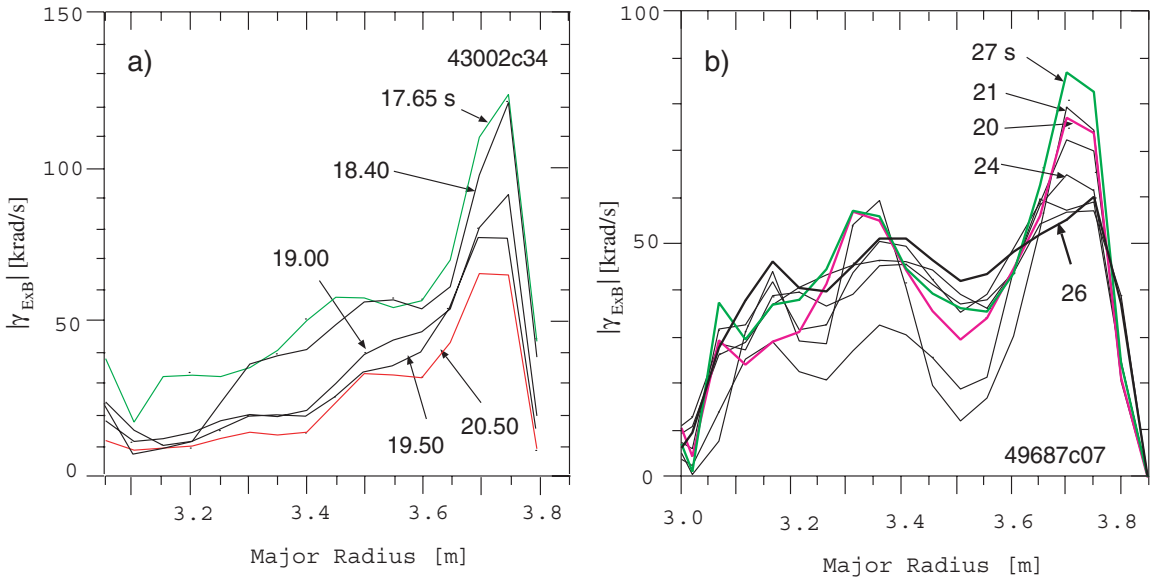

Figure 9. Shearing rate.

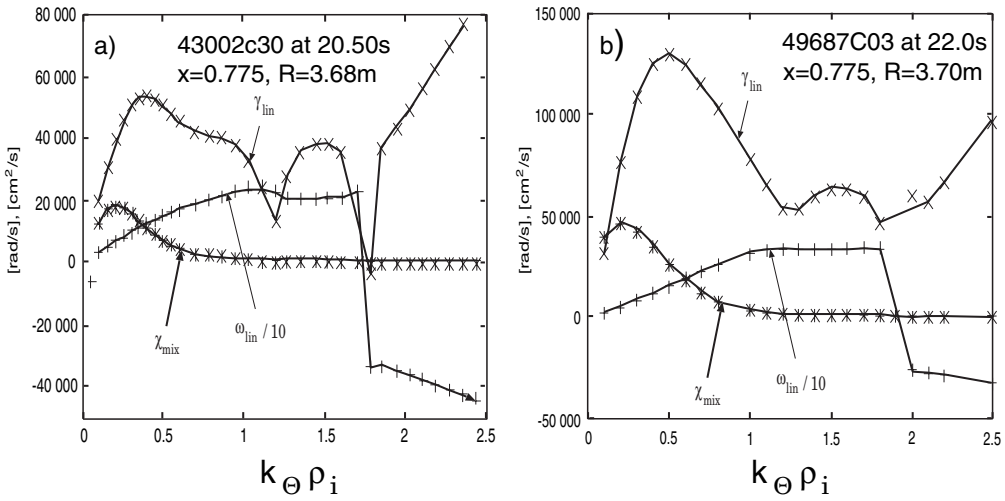

Figure 10. Spectra of γ_{lin}, ω_{lin} and the mixing length estimate of χ_i at $x = 0.775$ ($R = 3.74$ m).

during the times of interest here.

The shearing rate on the outer midplane is given in terms of E_r [5] by

$$\gamma_{E\times B} = \left(\frac{R^2 B_{pol}^2}{B}\right) \frac{\partial}{\partial \psi} \left(\frac{E_r}{R B_{pol}}\right)$$
$$\simeq \left(\frac{R B_{pol}}{B}\right) \frac{\partial}{\partial R} \left(\frac{E_r}{R B_{pol}}\right). \quad (4)$$

The results for E_r shows little change in shape, with magnitude evolving in time similar to f_{tor}. $\gamma_{E\times B}$ peaks near the pedestal, as shown in Fig. 9. For 43002, the peak decreases by about a factor of 2 as the confinement degrades, while for 49687, the peak decreases by a smaller fraction.

5. Gyrokinetic analysis

Low frequency electrostatic drift type instabilities, driven by ion temperature gradient (ITG) and/or trapped electron mode (TEM) dynamics, are candidates for the anomalous transport generally observed in tokamak plasmas. We used the comprehensive electromagnetic GS2 code [21,22] to calculate the linear growth rate γ_{lin} and the real part of the mode frequency ω_{lin} for the fastest growing mode. GS2 is an initial value code which solves the linearized gyrokinetic equation in a general flux tube geometry. A new TRANSP postprocessor generates the GS2 inputs [23]. We included up to seven species: thermal electrons, thermal hydrogenic ions, one impurity and the fast ions from the NBI.

GS2 assumes a fixed product of the poloidal mode number k_θ ($= nq/r$ in the circular approximation) and the ion gyroradius ρ_i. Ranges of values for $k_\theta \rho_i$ were scanned at each time zone to maximize γ_{lin}. Plots of the spectra at two time zones during the reduced confinement phases of the plasmas are shown in Figs 10 and 11. At low, values of $k_\theta \rho_i$ (<1), γ_{lin} has a broad peak versus $k_\theta \rho_i$ with a maximum value at around $k_\theta \rho_i = 0.30$–0.50. This value is around the values typically found in gyrokinetic and gyrofluid simulations [24]. The mode

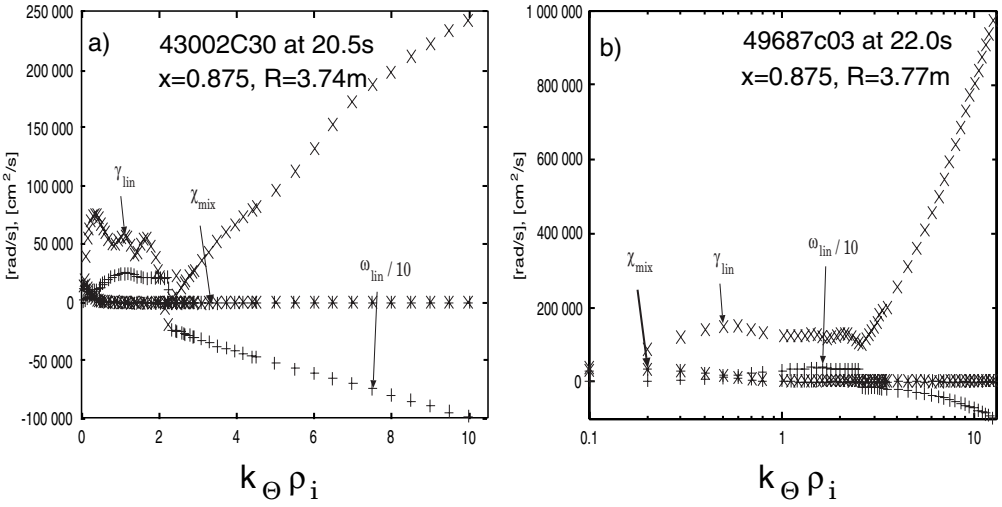

Figure 11. Spectra of maximum growth rate γ_{lin}, mode frequency ω_{lin} and the mixing length estimate of χ_i at $x = 0.875$ ($R = 3.77$ m).

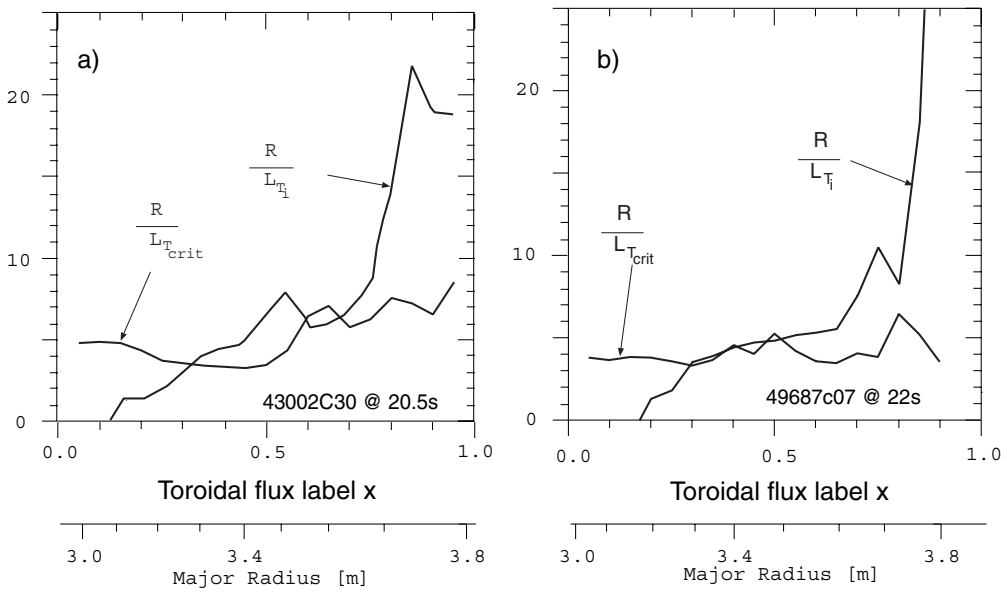

Figure 12. Comparison of R/L_{Ti} and R/L_{crit} estimated using the IFS–PPPL model versus toroidal flux label.

frequency ω_{lin} is positive (in the ion diamagnetic direction), which is typical of the ITG branch. At larger values of $k_\theta \rho_i$, ω_{lin} changes sign and the TEM branch dominates. The ITG and TEM branches can interact non-linearly, but we have not studied that interaction.

The 'mixing length' estimate of χ_i is also shown in Figs 10 and 11. This is defined by

$$\chi_{mix} = \gamma_{lin}/(k_\theta^2 + \langle k_r^2 \rangle) \tag{5}$$

where $\langle k_r^2 \rangle$ is the flux tube average of the computed radial k_r. χ_{mix} peaks at low values of $k_\theta \rho_i$ for both plasmas, suggesting that low $k_\theta \rho_i$ modes cause most of the anomalous transport. For this reason, we used the lower values of γ_{lin} from the ITG branch in this article.

The measured T_i gradients are compared with the IFS–PPPL model [25] estimate of the critical value in Fig. 12. Near the midradius of both plasmas, the major radius normalized gradient R/L_{Ti} is close to the critical value R/L_{crit}. The IFS–PPPL model was calibrated in the core, not the edge or pedestal, and was calibrated for the ITG branch, not the TEM branch.

Generally γ_{lin} is positive over a significant portion of the major radius near the outer midplane. Both $\gamma_{E\times B}$ and γ_{lin} peak near the top of the pedestal, as shown in Fig. 13. At the region of peak γ_{lin}, $\gamma_{E\times B}/\gamma_{lin}$ is of order 0.5–2.0, as shown in Fig. 1. Deeper in the plasma (near the midradius) a state of marginal stability is maintained in the sense that γ_{lin} and χ_i depend sensitively on R/L_{Ti}, which is close to its critical value. This is consistent with the observation that χ_i remains larger than approximately five times the neoclassical level over a wide range of densities and operating conditions. For 49687 with a wider variation in confinement, $\gamma_{E\times B}/\gamma_{lin}$ decreases to relatively low values and then recovers when the confinement recovers.

Profiles of γ_{lin} at various times are shown in Fig. 14. For 43002, γ_{lin} is relatively constant in time, decreasing only

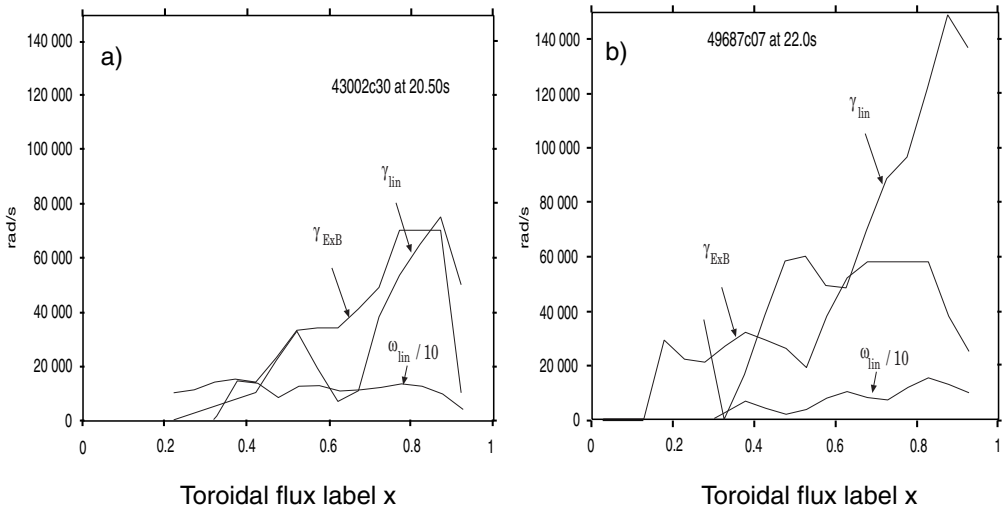

Figure 13. Profiles of γ_{lin}, ω_{lin} and $\gamma_{E\times B}$ at a time (2.20 s) during the low confinement phase.

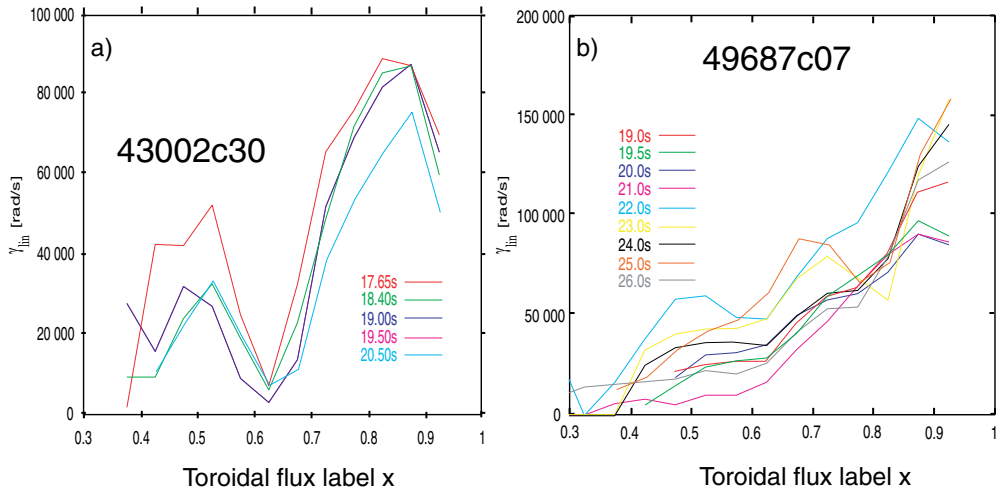

Figure 14. Profiles of γ_{lin} at different times.

slightly. The reduction in $\gamma_{E\times B}$ causes the ratio $\gamma_{E\times B}/\gamma_{lin}$ to decrease by roughly 20% near the top of the pedestal, as the global confinement decreases by roughly 20%. For 49687, γ_{lin} increases considerably while $\gamma_{E\times B}$ remains relatively constant; thus $\gamma_{E\times B}/\gamma_{lin}$ is reduced.

6. Summary and discussion

The transport and microinstability have been analysed for two JET ELMy H mode plasmas with degradation of confinement associated with the transition from the type I to the type III ELMy phase. The ion and effective heat conduction transport coefficients increase as the global and local energy confinement degrades. We calculated E_r using the measured carbon temperature and toroidal rotation rate, and estimating the poloidal rotation using neoclassical theory. The magnitude of $\gamma_{E\times B}$ calculated from E_r has a peak near the top of the pedestal which decreases with confinement.

The gyrokinetic simulations show that the plasmas are unstable to the ITG/TEM/ETG modes, but the linear growth rates of the ITG modes are comparable to the growth of the flow shearing rate. For 43002, the growth rate γ_{lin} of the fastest growing mode is relatively constant while $\gamma_{E\times B}$ decreases, but $\gamma_{E\times B}$ remains larger than or comparable to γ_{lin}. The degradation of energy confinement and increase in local heat transport with increasing density are correlated with a slight decrease in the ratio $\gamma_{E\times B}/\gamma_{lin}$. For 49687, $\gamma_{E\times B}$ remains relatively constant while γ_{lin} increases significantly, causing a large decrease in $\gamma_{E\times B}/\gamma_{lin}$, consistent with the significant loss of confinement. Thus the criterion for reduction of the microturbulence, $\alpha_{exb}\gamma_{E\times B} \simeq \gamma_{lin}$, with $\alpha_{exb} \simeq 0.5$–2.0 (Eq. (1)) appears to be applicable to this plasma within 10–15 cm of the top of the pedestal.

Other effects could contribute to the decrease in local energy confinement and increase in transport. For instance, the collisionality in the edge increases for 43002 and decreases for 49687. This contrasts with the observation that in JET H mode plasmas the edge collisionality generally increases at the transition from type I to III ELMs [4]. Recent non-linear gyrokinetic simulations indicate that increasing collisionality damps the zonal flows that also contribute to reducing turbulence [26], so increased collisionality is predicted to lead

to increased transport. As yet, we have not calculated this effect.

The ELMs affect the pedestal, and their effects might extend further inward. The gyrokinetic analysis indicates unstable modes peaking at around 3.7 m, about 10 cm inside the pedestal, but also extending inward to 3.3 m. It is unlikely that the ELMs could have a direct (local) effect this deep in the plasma. However, changes in the pedestal will affect the gradients, causing changes in confinement, although the GS2 analysis is non-local in the poloidal direction, it is local in the radial direction, depending only on local plasma parameters such as T_i, and gradients. Thus the indirect effects in the core of ELMs and pedestal changes are modelled as local effects.

The peak in $\gamma_{E\times B}$ could be the cause of the pedestal and consequently of the ELMs. The large values of $\gamma_{E\times B}$ found near the top of the pedestal increase the $\gamma_{E\times B}/\gamma_{lin}$ suppression of transport, leading to a transport barrier. This barrier causes a pile-up of stored energy, increasing the energy density near the top of the pedestal. The energy that does leak out cascades down the pedestal either at a steady state rate, or intermittently, with ELMs.

Our results linking $\gamma_{E\times B}/\gamma_{lin}$ with increased transport and degradation of confinement suggest that tokamak reactors which rely on high density and high energy confinement in the ELMy H mode may require a source of torque to maintain a high $\gamma_{E\times B}/\gamma_{lin}$, at least near the top of the pedestal. It may prove more effective to drive poloidal than toroidal rotation since E_r and $\gamma_{E\times B}$ are generated by the sum $v_{pol}B_{tor} - v_{tor}B_{pol}$, although poloidal rotation is thought to be highly damped. It may be sufficient to apply a torque dipole near the top of the pedestal to generate large $\gamma_{E\times B}$.

Acknowledgements

We wish to thank the members of the JET team for the excellent data and W. Dorland for help with the GS2 code. This work was supported in part by US Department of Energy contract DE-AC02-76CH03073.

References

[1] Horton, L.D., et al., Nucl. Fusion **39** (1999) 993.
[2] Saibene, G., et al., Nucl. Fusion **39** (1999) 1133.
[3] Horton, L.D., JET Team, in Fusion Energy 2000 (Proc. 18th Int. Conf. Sorrento, 2000), IAEA, Vienna (2001) CD-ROM file EX2/1 and http://www.iaea.org/programmes/ripc/physics/fec2000/html/node1.htm.
[4] Chankin, A., Saibene, G., Plasma Phys. Control. Fusion **41** (1999) 913.
[5] Hahm, T.S., Burrell, K.H., Phys. Plasmas **2** (1995) 1648.
[6] Waltz, R.E., Kerbel, G.D., Milovich, J., Phys. Plasmas **1** (1994) 2229.
[7] Beer, M.A., et al., in Controlled Fusion and Plasma Physics (Proc. 26th Eur. Conf. Maastricht, 1999), Vol. 23J, European Physical Society, Geneva (1999) 1669.
[8] Synakowski, E.J., et al., Phys. Rev. Lett. **78** (1997) 2972.
[9] Shirai, H., et al., Plasma Phys. Control. Fusion **42** (2000) A81.
[10] Ernst, D.R., Coppi, B., Scott, S., Porkolab, M., TFTR Group, Phys. Rev. Lett. **81** (1998) 2454.
[11] Synakowski, E.J., et al., Nucl. Fusion **39** (1999) 1733.
[12] La Haye, R.J., et al., Nucl. Fusion **35** (1995) 988.
[13] Budny, R.V., et al., Phys. Plasmas **7** (2000) 5038.
[14] Budny, R.V., JET Team, in Fusion Energy 2000 (Proc. 18th Int. Conf. Sorrento, 2000), IAEA, Vienna (2001) CD-ROM file EXP5/19 and http://www.iaea.org/programmes/ripc/physics/fec2000/html/node1.htm.
[15] Gowers, C., et al., Rev. Sci. Instrum. **66** (1995) 471.
[16] von Hellermann, M., Summers, H., in Atomic and Plasma Material Interaction Processes in Controlled Thermonuclear Fusion, Elsevier, Amsterdam and New York (1993) 135.
[17] Hawkes, N., Peacock, N., Rev. Sci. Instrum. **63** (1992) 5164.
[18] Budny, R.V., et al., Nucl. Fusion **35** (1995) 1497.
[19] Houlberg, W., Shaing, K., Hirshman, S., Zarnstorff, M., Phys. Plasmas **4** (1997) 3230.
[20] Ernst, D., et al., Phys. Plasmas **5** (1998) 665.
[21] Dorland, W., et al., in Fusion Energy 2000 (Proc. 18th Int. Conf. Sorrento, 2000), IAEA, Vienna (2001) CD-ROM file TH2/5 and http://www.iaea.org/programmes/ripc/physics/fec2000/html/node1.htm.
[22] Kotschenreuther, M., Rewoldt, G., Tang, W., Comput. Phys. Commun. **88** (1995) 128.
[23] Ernst, D.R., et al., Phys. Plasmas **7** (2000) 615.
[24] Dimits, A.M., et al., Phys. Plasmas **7** (2000) 969.
[25] Kotschenreuther, M., Dorland, W., Beer, M., Hammett, G., Phys. Plasmas **2** (1995) 2381.
[26] Lin, Z., Hahm, T., Lee, W., Tang, W., Diamond, P., Phys. Rev. Lett. **83** (1999) 3645.